View Article Online
View Journal

Green Chemistry

Cutting-edge research for a greener sustainable future

Accepted Manuscript

This article can be cited before page numbers have been issued, to do this please use: S. Yoon, C. Bateman, J. J. Busfield, P. Martin and B. Chen, *Green Chem.*, 2026, DOI: 10.1039/D6GC00989A.

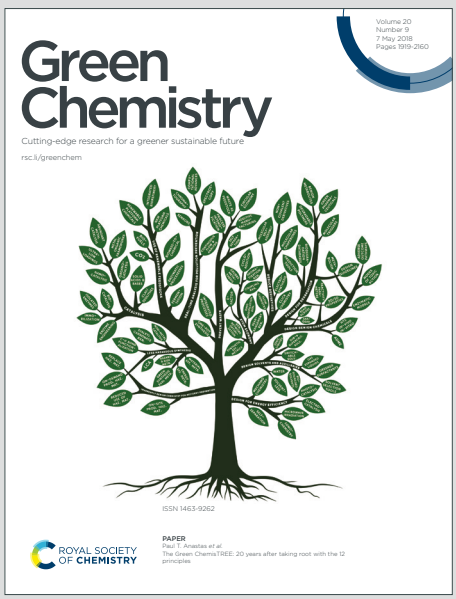

View Article Online
DOI: 10.1039/D6GC00989A

Green Foundation

1. This work synthesises biobased long-chain polyether diols using a green scalable method, enabling flexible molecular designs of ether-based thermoplastic elastomers.
2. Different types of biobased thermoplastic elastomers with a broad range of controllable properties were synthesised from these long-chain polyether diols. They are promising sustainable alternatives to some existing fossil-based thermoplastic elastomers and vulcanised rubbers in various applications.
3. Specialty tests of these renewable thermoplastic elastomers may be carried out in the future to fully assess their potential for targeted applications, and where necessary optimisation of the material composition may be conducted to achieve desirable properties.

View Article Online
DOI: 10.1039/D6GC00989A

ARTICLE

A Green Versatile Platform for Synthesising Renewable Ether-Based Thermoplastic Elastomers

Received 00th January 20xx,
Accepted 00th January 20xx

DOI: 10.1039/x0xx00000x

Sungkwon Yoon[a], Charlie Bateman[a,b], James J. C. Busfield[c], Peter J. Martin[a], and Biqiong Chen*[,a,b]

Ether-based polymers are commonly used in diverse applications. However, it is challenging to synthesise polyethers with more than five methylene groups in their main chains, which limits the molecular design of ether-based polymers. Creating a new synthesis pathway to enabling green chemistry and flexible design of their molecular structures is, therefore, highly desired. Here, a green versatile platform is presented for synthesising renewable ether-based thermoplastic elastomers (TPEs) with broad and tuneable properties. An organic acid catalyst is used to synthesise a long-chain polyether diol from a fatty acid diol *via* a S_N2 reaction. This biobased, renewable polyether diol then serves as a universal platform for the synthesis of a wide spectrum of TPEs including thermoplastic polyurethanes, poly(urethane urea)s and poly(ether ester) elastomers, with controllable mechanical properties, excellent transparency and chemical resistance. The structure-property relationships, processability, and sustainability of these TPEs are also reported. The synthesis of these biobased TPEs can be readily scaled up, and different types of products are manufactured from the elastomers. This work provides a viable synthesis strategy to overcoming the limitations of the molecular design facing existing ether-based polymers, while enabling the sustainable manufacture of renewable ether-based TPE materials and products.

Introduction

Biobased polymers are receiving increasing interest in the development of sustainable alternatives to fossil-based polymers, due to their renewability. A broad range of biobased renewable polymers such as thermoplastic elastomers (TPEs) and rigid plastics have been produced.[1–3] Ether-based polymers are often found in various applications, because of their high chemical stability and flexibility in incorporating other chain segments.[4,5] They are commonly prepared by ring-opening polymerisation (ROP) of cyclic ethers, with metal hydroxides or metal cyanides as catalysts.[6] However, this method cannot prepare polyethers containing six or more methylene units, due to the exceptional chemical stability of cyclic ethers [6], significantly limiting the variety of the main-chain structure and molecular design in the final polyethers and ether-based polymers. Furthermore, the use of metal catalysts may cause issues like high costs, environmental concerns, and limitations of application in food contacts and healthcare.[7]

Williamson ether synthesis can achieve polyether diols with longer methylene units, in which a nucleophilic substitution of an alkoxide with a halogenated alkane is performed.[8] However, generation of toxic halogen compound byproducts is often inevitable. The oxa-Michael reaction does not inherently generate hazardous byproducts, but usually requires Michael acceptors such as acrylonitrile, methyl acrylate and acrylamide which are carcinogenic or irritant.[9] Moreover, this reaction often suffers from side reactions with cyclic byproducts and radical homopolymerisation yielding polyacrylates instead of polyethers.[10] Polyethers have also been produced by direct polycondensation of alcohols with acid catalysts such as sulfuric or sulfamic acid, and water as the byproduct.[6] However, ionic liquids with high temperature stability are often required to carry these catalysts to withstand the elevated temperatures during polycondensation.[11] Due to the high costs of ionic liquids, this method is considered commercially inviable. Noneutectic or eutectic organic acid and base catalyst systems have been introduced to tackle this issue,[12,13] but the reaction frequently leads to undesirable low molecular weights after a relatively long synthesis time (e.g., <1500 g mol^{-1}, 48 h),[12] or byproducts from the organic base that requires a further purification process.[13] So a green and cost-effective route to synthesising polyether diols with long chains and controllable molecular structures, is highly demanded for the production of polyethers, with no metal catalysts and halogen byproducts involved.

Here, we present a green, versatile and cost-effective platform for synthesising renewable ether-based TPEs with a broad range of tuneable properties. A long-chain polyether diol was successfully synthesised from a sustainable dimerised and hydrogenated fatty

[a] School of Mechanical and Aerospace Engineering, Queen's University Belfast, Stranmillis Road, Belfast, BT9 5AH, United Kingdom
[b] Department of Chemistry, University of Liverpool, Crown Street, Liverpool, L69 7ZD, United Kingdom. Email: biqiong.chen@liverpool.ac.uk
[c] School of Engineering and Materials Science, Queen Mary University of London
Mile End Road, London, E1 4NS, United Kingdom

Supplementary Information available: additional characterisation methods, additional GPC, FTIR, NMR, DSC, XRD, UV-vis, TGA, DMA, mechanical and rheological testing results, as well as process modelling, processing and product

acid diol with 36 carbons (Pripol™ 2030), by direct polycondensation using an organic acid catalyst, *p*-toluenesulfonic acid (PTSA), in a bulk, kilogram-scale production with water only as the byproduct. PTSA has a relatively high thermal degradation onset temperature (~200 °C, under inert gas).[14] Combining the use of the long-chain fatty acid diol and the thermally stable PTSA, polyether diols with a desirably high methylene number and molecular weight were achieved. Thermoplastic polyurethanes (TPUs) with rational designs of molecular structure were prepared from this biobased long-chain polyether diol to achieve a wide spectrum of properties for diverse potential applications. Their property tuneability and versatile processability, as well as the generalised synthesis method for other TPEs including poly(urethane urea)s (PUUs) and poly(ether ester) elastomers (TPEEs), were demonstrated. Broadly, this work offers great flexibility for the sustainable design and synthesis of polyethers and ether-based TPEs.

Results and Discussion

Synthesis of Long-Chain Polyether Diols

Long-chain polyether diols were synthesised from Pripol 2030 by an S_N2 or biomolecular nucleophilic substitution reaction using PTSA as the catalyst (Fig.s 1a-b and Supplementary Information Fig. S1). Here, the hydroxyl end groups in Pripol 2030 react each other to form ether linkages with water as the byproduct. Formation of ether bonds is confirmed by nuclear magnetic resonance (NMR) and Fourier transform infrared spectroscopy (FTIR) (Fig.s 1c-e, S2 and S3). The CH_2 proton bonded with ether (C–O–C) linkages appears at 3.4 ppm, the proton of hydroxyl (O–H) end groups at 3.7 ppm (^{1}H NMR, Fig. 1c),[15] the deshielded carbon from C–O–C at 71 ppm, carbon adjacent to hydroxyls at 63 ppm (^{13}C NMR, Fig. 1d), and C–O–C stretching vibration peak at 1117 cm^{-1} (FTIR, Fig. 1e).[15,17]

The number average molecular weight, $\overline{M}_n$, of polyether diols, determined by gel permeation chromatography (GPC), increases with synthesis time from 2200 ± 100 g mol^{-1} for 7 h to 4700 ± 200 g mol^{-1} for 19 h (Fig. S4 and Table S1). These $\overline{M}_n$ values are equivalent to 76 and 163 carbons (CH_2 and CH) on the main chain of polyether diols (with additional carbons on side chains), addressing the current challenge associated with producing polyether diols of more than five methylene units and offering the flexibility in designing the length of the main chain. The results also show a low batch-to-batch variation of less than 5%, giving evidence of good reproducibility.

Design and Synthesis of Ether-based Thermoplastic Polyurethanes

Ether-based TPUs were investigated as the main model family of TPEs in this work, owing to their segmented copolymer structure that consists of alternating soft segments and hard segments allowing for flexible design of molecular structures. The new biobased long-chain polyether diol acts as the soft segment, while the hard segment is the product of a chain extender reacting with an excess diisocyanate (molar ratio of isocyanate to hydroxyl groups = 1.1:1) to compensate self-oligomerisation of diisocyanates (Fig.s 2a and S5).[18] 1,4-cyclohexanedimethanol (CHDM) was selected as the chain extender for good optical clarity due to its ability to disrupt anisotropic ordering and suppress birefringence,[19] as well as for enhanced hydrolysis resistance because of its bulky, cyclic structure.[20]

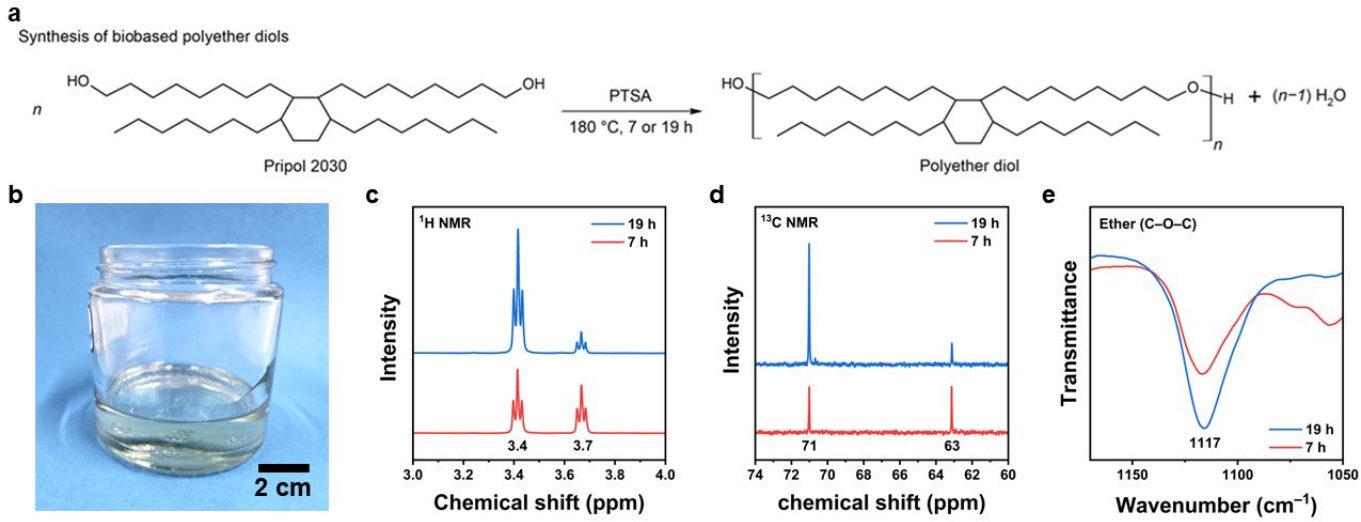

Fig. 1 Synthesis and chemical structure of biobased long-chain polyether diols. a, Chemical reaction scheme showing the synthesis of the biobased polyether diols. The chemical structure presented for Pripol 2030 only illustrates one possible structure. b, A photograph showing a biobased polyether diol with a synthesis time of 19 h. c, ^{1}H NMR spectra showing the CH_2 proton bonded with ether (C–O–C) linkages. d, ^{13}C NMR spectra showing a peak associated with the deshielded carbon from C–O–C. The NMR spectra were shifted vertically for visual clarity. e, FTIR spectra showing the C–O–C stretching vibration peak.

View Article Online
DOI: 10.1039/D6GC00989A

ARTICLE

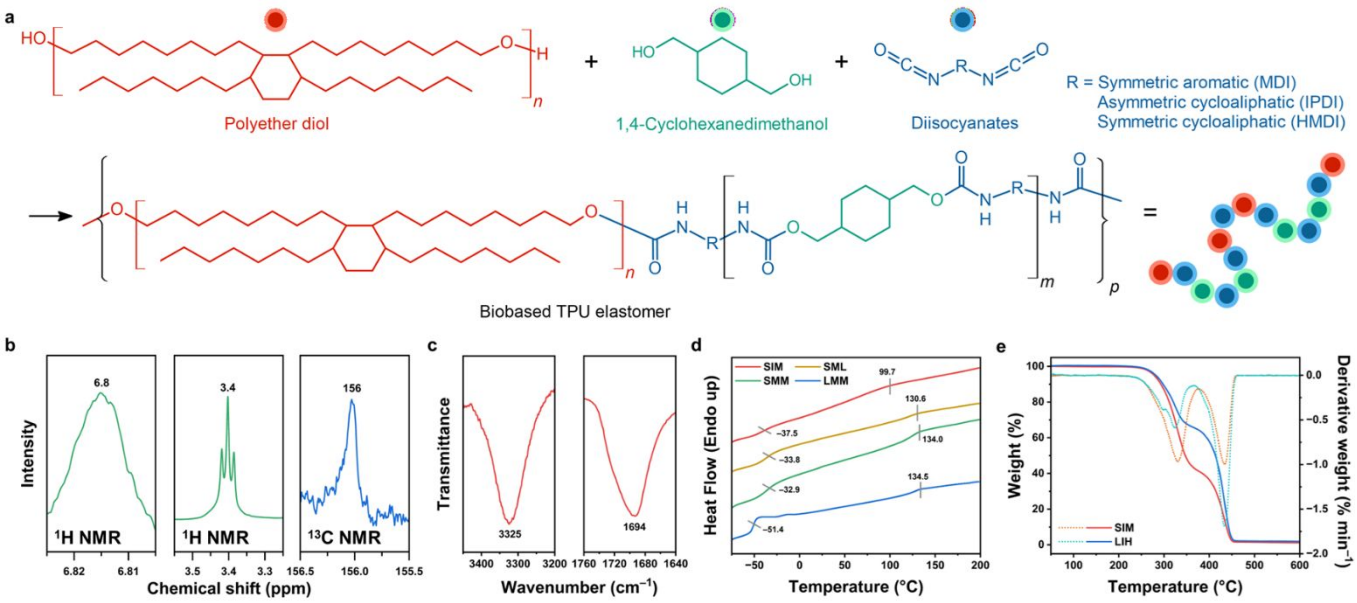

Fig. 2 Characteristics of ether-based TPU elastomers. a, Chemical reaction scheme showing the synthesis of TPUs using the new biobased long-chain polyether diols. b, ^{1}H and ^{13}C NMR spectra affirming the formation of urethane linkages in TPUs. c, FTIR spectra showing urethane peaks of TPUs. d, DSC 2nd heating curves and e, TGA curves revealing the thermal transition characteristics of TPUs.

Asymmetric cycloaliphatic isophorone diisocyanate (IDPI), symmetric aromatic 4,4'-methylenebis(phenyl isocyanate) (MDI) and symmetric cycloaliphatic 4,4'-methylenebis(cyclohexyl isocyanate) (HMDI) were used as diisocyanates to achieve different properties. The hydroxyl groups of the soft segment react with the isocyanate groups of the hard segment, yielding TPUs (Fig. S5). Sample codes of TPUs are presented as XYZ, where X represents the synthesis time of the polyether diols used (S for short 7 h or L for long 19 h), Y is the diisocyanate species (I for IPDI, M for MDI and H for HMDI), and Z indicates the relative molar ratio of hard segment to soft segment (L for low, M for medium and H for high) (Table S2).

Formation of TPUs is confirmed by the presence of new urethane bonds under NMR and FTIR (Fig.s S6 and S7). The urethane N–H and CH_2–O proton peaks appear at 6.8 ppm and 3.4 ppm, respectively (^{1}H NMR, Fig. 2b).[21,22] The urethane C=O carbon peak appears at 156 ppm (^{13}C NMR, Fig. 2b).[23] FTIR (Fig. 2c) affirms the urethane amide A (N–H stretching, 3325 cm^{-1}) and amide I (C=O stretching, 1694 cm^{-1}).[15,24,25] The absence of isocyanate group is confirmed by FTIR, indicating full conversion into urethane bonds.[26]

$\overline{M}_n$ of the TPUs varies with the synthesis formulation, ranging from 10,100 to 32,200 g mol^{-1}, with polydispersity index (PDI) between 2.42 and 3.18 (Fig. S8 and Table S3). These $\overline{M}_n$ values are similar to or lower than those reported for existing TPUs (which are typically in the range of 19,700 – 45,300 g mol^{-1}).[27,28] When MDI is used, $\overline{M}_n$ becomes higher, compared to the other two diisocyanates, because the charge resonance stabilisation of the aromatic rings in MDI provides higher reactivity and more extensive chain growth.[21,29] The PDI over 2 originates from the branched structure in the polyether diols,[17] and the non-stoichiometric ratios between isocyanate and hydroxyl groups.[18]

The new biobased TPUs are transparent or translucent, and are mostly amorphous (with very small and broad melting peaks from differential scanning calorimetry, DSC) (Fig.s 2d and S9–11), attributable to their irregular or branched chain structure predominantly arising from the soft segments with side chains. Depending on the structure and molecular weight, the melting temperature of the TPUs ranges from 88.6 to 141.4 °C. Despite the dominant amorphous structures, these TPUs have excellent resistance to water of different pH values (acidic pH 3.8, neutral pH 6.8 and basic pH 9.8) (weight changes of no more than ±1% after 7 days' immersion) (Fig. S12 and Table S4). This high hydrophobicity is mainly due to the long and branched hydrophobic methylene chain segments in the soft segments as well as the bulky aromatic or cycloaliphatic structures in the hard segments.[30,31] Some of these TPUs also show excellent resistance to hydrocarbon oils (<5% absorption of mineral oil after 7 days' immersion), especially when a higher hard segment ratio is used with increasing polar urethane linkages.

The TPUs exhibit glass transition temperatures, T_g, between −51.4 °C and −37.5 °C (from mid-point of DSC) (Fig.s 2d, S10 and Table S5), confirming their rubbery behaviour at ambient temperature (~20 °C). In general, increasing the length and/or molar ratio of the soft segment leads to a lower T_g while changing the hard segment from a cycloaliphatic to a more rigid aromatic diisocyanate gives rise to a higher T_g. Compared to their asymmetrical counterparts, symmetrical diisocyanates result in higher T_g on account of the formation of stronger intermolecular hydrogen bonding between the hard segments.[32]

The biobased TPUs show good thermal stability, with the first onset thermal degradation temperature (T_{d1}^{onset}) (measured by thermogravimetric analysis, TGA), between 266.5 – 295.9 °C due to the initial degradation of the hard segments through cleavage of urethane bonds (Fig.s 2g, 13 and Table S6).[32,33] This T_{d1}^{onset} is higher when compared to some existing ether-based TPUs (200 – 230 °C).[34,35] The second onset thermal degradation (T_{d2}^{onset}) between 400.2 – 428.4 °C is attributable to the degradation of the soft segments,[36] which again is higher than existing TPUs (300 – 380 °C),[35,37] possibly due to the ample van der Waals interactions between the branched and long methylene chains in the soft segments.[17,32,38] The two distinctive degradation behaviours in a TPU indicates well-defined phase separation structures between the soft and hard segments.[32] These high T_ds ensure the processing flexibility by reducing the risk of polymer decomposition during manufacturing processes.[39]

Tuneable Mechanical Properties of Ether-based Thermoplastic Polyurethanes

The new biobased TPUs are flexible and stretchable, withstanding repeated twisting and stretching (Fig. 3a). Their mechanical properties are tuneable by varying the composition of the building blocks, e.g., the chain length of the soft segment, the chemical structure of the hard segment, and the molar ratio of the soft segment, chain extender and diisocyanate.

By using the shorter polyether diol as the soft segment (S-series samples), the tensile stress at 15% strain, tensile strength, and hardness of the resulting TPUs increase over those with the longer polyether diol (L-series samples), reaching 16.67 ± 1.15 MPa, 20.36 ± 1.30 MPa, and 67.3 ± 1.7 (Shore D) (Fig.s 3b, 14 and Table S7). The L-series TPUs show lower stress at 15% strain, tensile strength, and hardness values, as low as 0.19 ± 0.02 MPa, 5.68 ± 0.28 MPa and 50.7 ± 1.2 (Shore A), as well as higher elongation at break up to 791 ± 23% (Fig.s 3c, 15 and Table S8). These results are mainly attributable to the lower molar ratios of the hard segment in the TPUs. The TPUs with aromatic and symmetric hard segment (from MDI) show higher tensile strength and hardness than those with asymmetric cycloaliphatic hard segment (from IPDI) due to the presence of rigid aromatic rings and the stronger hydrogen bonding between macromolecular chains in symmetric structures.[32]

The L-series TPUs are highly elastic with no obvious yield during tensile testing (Fig. 3c), and low hysteresis during cyclic loading up to 100% strain (Fig. 3d) reaching as low as 0.116 for the 100th cycle (Fig. S16 and Table S9). Notably, there is a synergistic effect of the higher degree of physical crosslinking with aromatic and symmetric hard segment providing higher elasticity, and the soft segment with higher methylene numbers providing better chain flexibility. Their compression sets are also lower than most of existing TPUs (10 – 50%),[40,41] measuring as low as 5.7% (after 24 h) or 13.6% (after 72 h) (Fig. 3e).

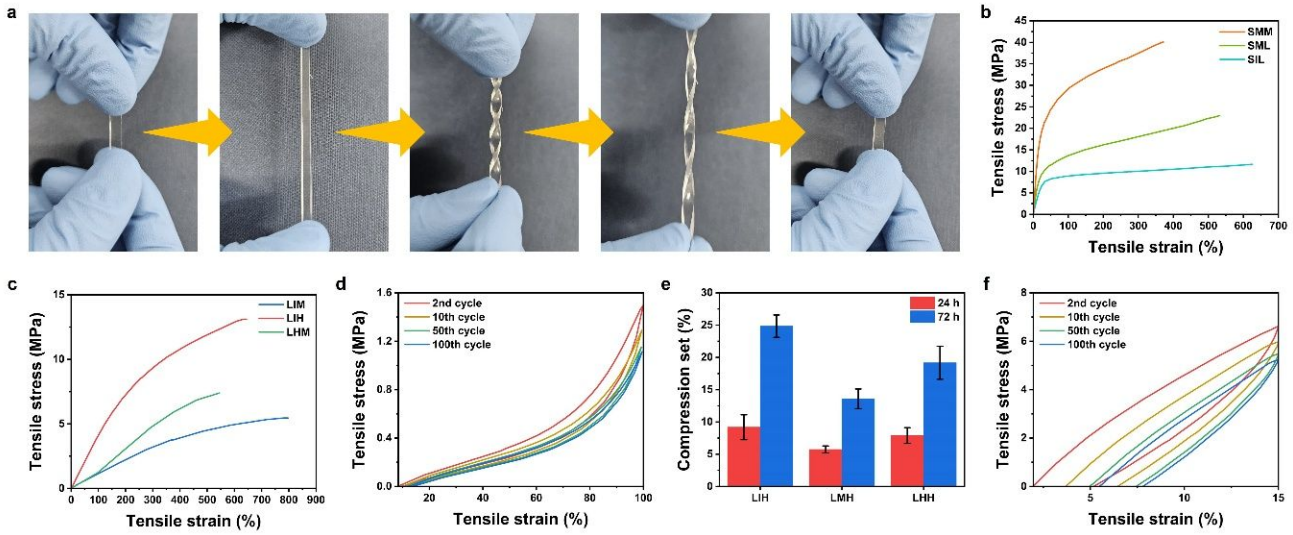

Fig. 3 Tuneable mechanical properties of ether-based TPUs demonstrated by tensile, compression set, and cyclic tensile testing. a, Demonstration of stretchability and flexibility of TPUs by stretching and twisting a TPU strip. b, c, Representative tensile stress-strain curves of TPUs using (b) the shorter polyether diol soft segment (S-series samples), and (c) the longer polyether diol soft segment (L-series samples). d, A cyclic tensile stress-strain curve of a TPU using the longer polyether diol (LMM) after the first preconditional cycle. e, compression set measured from the L-series TPUs. f, A cyclic tensile stress-strain curve of a TPU using the shorter polyether diol (SML) after the first preconditional cycle.

View Article Online
DOI: 10.1039/D6GC00989A

ARTICLE

Similarly, the highly flexible soft segment of the biobased polyether diol with high carbon numbers helps the TPUs deform during compression, and the high degree of physical crosslinking in the TPUs facilitates shape recovery after compression. In contrast, some of the S-series TPUs experience yield between 26.8 ± 2.5% and 28.3 ± 5.4% strain (Fig. 3b) and relatively high hysteresis or energy dissipation (Fig. 3f) (Fig. S16 and Table S9), due to the bulky cycloaliphatic hard segment structures, providing steric repulsions and eventual chain stiffness at the relatively high hard segment contents.[42]

Viscoelastic and Die Swell Behaviour of Ether-based Thermoplastic Polyurethanes

Dynamic mechanical analysis (DMA) and rheological testing were carried out to evaluate the viscoelastic and die swell behaviour of TPUs. DMA results (Fig.s 4a–b and S17) show the storage modulus of all the tested TPUs is above loss modulus across the test temperature range, suggesting the materials behave predominantly as a solid and confirming their elastomer characteristic.[43] When the chain length and molar ratio of the soft segment are fixed, varying the diisocyanate influences the storage modulus in the order of IPDI > HMDI > MDI. The loss factor for the tested S-series TPUs is higher than that of the tested L-series TPUs, implying their higher damping and energy dissipation.[43] T_g values of all the tested TPUs (from the peak temperature of *tanδ*) were observed between –23.9 and –19.3 °C, confirming soft segment dominance in the TPUs[45].

The rheological characterisation of representative TPUs (Fig.s 4c–d and S18) reveals their different viscoelastic behaviours at the test temperature 140 °C: LHH shows predominantly elastic response at frequencies above 0.1 rad s^{-1}, while SIM exhibits mainly viscous behaviour across the test frequencies (0.05 – 628 rad s^{-1}) due to their contrasting molecular structures. Furthermore, LHH shows highest shear storage modulus among the tested samples (Fig. S18), implying its highest die swell during extrusion. The long-chain polyether diol results in a TPU with a higher shear storage modulus (LIM) than that with the short-chain polyether diol (SIM). The complex viscosity of all the tested samples demonstrates significant shear-thinning, an important property for the melt to flow during processing, with LHH showing the highest values across the test region (Fig. S18).

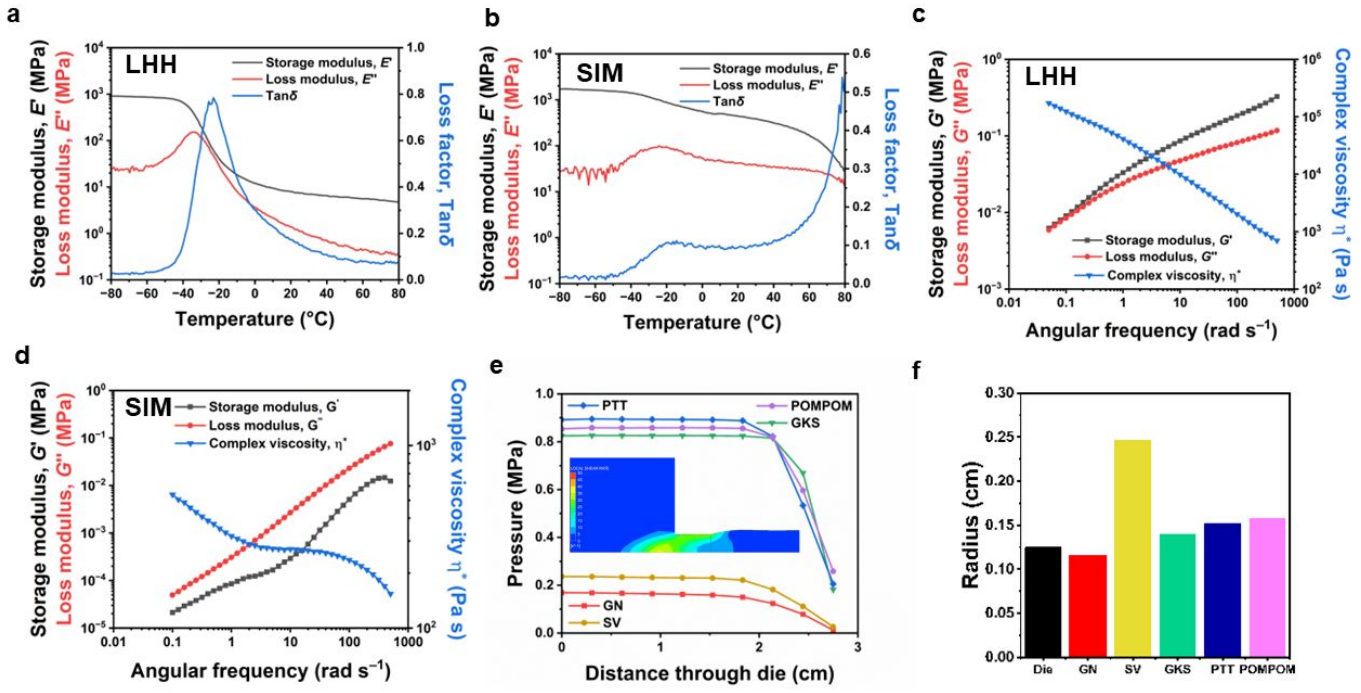

Fig. 4 Viscoelastic and die swell behaviour and extrusion modelling of ether-based TPUs. DMA curves of a, LHH and b, SIM TPUs. Rheology data of c, LHH and d, SIM TPUs. Simulation results of die swell using five mathematical models on LHH melt: e, pressure drop (inset picture represents the viscoelastic PTT model showing the plug effect as the polymer moves from the reservoir into the die and increased local shear rate; blue and red colours represent low and high shear rates, respectively) and f, increase in radius of extruded filament relative to the original die size taken from five mathematical models

View Article Online
DOI: 10.1039/D6GC00989A

ARTICLE

The viscoelastic behaviour and die swell of TPU melts were also studied by numeric simulations using ANSYS Polyflow with a die of internal diameter of 2.5 mm and five commonly used mathematical models: generalised Newtonian (GN), simplified viscoelastic (SV), Giesekus (GSK), Phan-Thien Tanner (PTT) and Pom-Pom (POMPOM).[46–48] Among these models, the GN model only considers viscous properties of polymer melts, while the other four are viscoelastic models which also account for the elastic properties. The viscoelastic models predict an elastic storage modulus and a viscous loss modulus. The GN and SV models prove to be the least accurate for simulating a biobased TPU melt, which treat the melt as a Newtonian fluid instead of a non-Newtonian, or shear thinning fluid. They significantly underestimated the pressure required during processing, and do not accurately display the non-linear pressure drop or realistic velocity profile for the TPU melt (Fig.s 4e and 19). In comparison, the more advanced viscoelastic models (GSK, PTT and POMPOM) provide a much more accurate representation of the viscoelastic behaviours of TPU melts. They predicted higher pressures with a sharp non-linear pressure drop at the die exit and a plug-flow velocity profile, which is characteristic of the shear-thinning and elastic stresses in polymer melts.[49] The GSK, PTT and POMPOM models give die swell values of 10%, 14% and 16% respectively for LHH (Fig. 4f). Similar die swell values of 14 and 18% were found for LIM and SIM using the PTT model (Fig. S20).

The melt flow index of the TPUs ranges between 6.0 and 18.9 g.10 min^{-1} (at 160 °C, 2.16 kg weight) (Table S10), which is higher than that of their petroleum counterpart (4.56 g 10 min^{-1} at 190 °C, 2.16 kg weight).[50] This can be attributed to its branched and amorphous structure which often leads to a low chain density with a higher flowability.[51] Branched polymer chain structure in the TPUs are known to form a "folded ball" structure that reduces hydrodynamic volume and has lower resistance to chain movement.

Versatile Processability of Ether-based Thermoplastic Polyurethanes

The new ether-based TPUs can be readily manufactured into different shapes using common polymer processing techniques such as extrusion, injection moulding, and compression moulding. Using a twin-screw extruder, TPU (LIH) tubes with varying inner and outer diameters of 1.14 – 6.05 mm and 1.74 – 7.77 mm were successfully produced (Fig.s 5a, 21 and Table S11). The tubing with an inner diameter of 2.96 mm and outer diameter of 3.88 mm shows a tensile strength and elongation at break of 15.3 ± 1.3 MPa and 288 ± 18% (Fig. S22), comparable to existing elastomer tubings.[52] Additionally, extrusion of these tubings was performed at a relatively low temperature (125 – 155 °C, owing to the lower melting point of TPUs (<141.4 °C) (Table S5) compared to commercial TPUs of similar Shore hardness (extrusion temperature ~200 °C),[34] which is beneficial for reducing energy consumption during polymer processing.

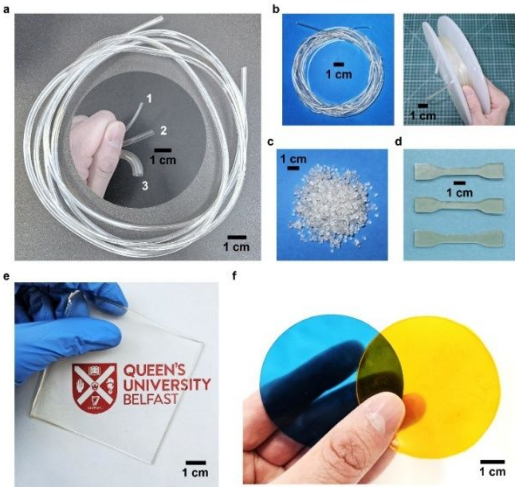

Fig. 5 Ether-based TPU elastomer products manufactured by common polymer processing techniques. a, TPU (LIH) elastomer tubings with three different inner and outer diameters (denoted as 1, 2 and 3) produced by extrusion. b, TPU (LHH) filaments for 3D printing: (left) as extruded and (right) rolled on a 3D printer wheel cartridge. c, TPU (LHH) pellets pelletised from filaments. d, Dumbbell (LHH) specimens by injection moulding. e, A hot-pressed TPU (LIH) film demonstrating its transparency. f, (Left) a blue-coloured TPU (LHH) film and (right) yellow-coloured TPU (LHH) film illustrating their dyeability.

Filaments (LHH) of a diameter of 1.75 ± 0.04 mm were also produced by extrusion (Fig. 5b) for potential applications including creating tailored flexible prototypes from 3D printing, and bulk production of TPU pellets (Fig. 5c). Dumbbell tensile test specimens were produced by injection moulding (Fig. 5d), and transparent film samples were prepared by hot pressing (Fig. 5e). The polymers can be dyed into different colours to alter their aesthetic appearance (Fig.s 5f and 23) showing good dyeability.

Generalised Synthesis Method for Other Ether-Based Elastomers

The green synthesis platform can be extended to other ether-based TPEs that contain long-chain polyethers, such as PUU and TPEE elastomers (Fig. S24, and Table S12). To synthesise PUUs, a polyether diol was polymerised with 1,6-hexamethylenediamine (HMDA) and IPDI, where the hydroxyl end groups of the polyether diol and primary amine end groups in HMDA reacted with the isocyanate groups in IPDI to form urethane and urea linkages, respectively. To synthesise TPEEs, 1,4-butanediol (BDO) and dimethyl terephthalate

View Article Online
DOI: 10.1039/D5GC00880A

(DMT) were used as the hard segment components, which reacted with the soft segment polyether diol by transesterification between the methyl ester group ($COOCH_3$) in DMT and OH end groups in the polyether diol and BDO.[53]

The chemical structure of the resulting biobased PUU and TPEEs is confirmed by NMR and FTIR (Fig. S25). The highly amorphous structure is confirmed by DSC (Fig. S26) and X-ray diffraction (Fig. S11). The elastomers show excellent water resistance (acid, neutral and basic, Fig. S12 and Table S4). They exhibit T_g values between –28.5 °C and –50.8 °C (by DSC), and the T_{d1}^{onset} values of 296.4 °C and 379.3 °C (Fig. S26 and Tables S13–14). The tensile properties of the PUU are within the range of TPUs described above. In contrast, the TPEE with the lower hard segment ratio (EEL) shows lowest tensile stress at 15% strain, tensile strength, hardness and highest elongation at break values, being 0.09 ± 0.01 MPa, 2.61 ± 0.23MPa, 32.3 ± 1.2 (Shore A) and 995 ± 65%, respectively (Fig. S27 and Tables S14–15), due to the highest soft segment ratio and presumably lowest interchain interactions because of the lack of hydrogen bonding.[53]

Sustainability of the Synthesis Method and the Synthesised Elastomers

The novel synthesis platform described here represents a green and universal approach to the synthesis of long-chain polyether diols without the use of a metal catalyst or the generation of harmful byproducts. Utilising these long-chain polyether diols, a broad spectrum of ether-based TPEs can be prepared. This synthesis can be readily scaled up for bulk production – using a laboratory set up, kilograms of TPEs were produced (Fig. S28). Due to the use of a long-chain fatty acid diol derived from renewable plant oils (Pripol 2030), the resulting TPEs contain biobased contents of 54.2 – 87.8 wt.%, which were calculated by the weight ratio of Pripol 2030 to the total amount of chemicals used to prepare each TPE. When a biobased chain extender and/or biobased diisocyanate is also used,[55–58] these TPEs can achieve up to 100% fully biobased contents (Fig. 6a). The thermoplastic nature of the elastomers makes the TPEs reprocessable and recyclable, showing no degradation in material colours and integrity after re-processing of the samples three times (data not shown). Furthermore, the new TPEs show low densities of 0.90 – 0.99 g cm^{-3} (Table S16), which are below 1 g cm^{-3} and useful in float separation process during recycling.[58]

These new renewable and recyclable ether-based TPEs possess comparable properties to some of existing biobased TPEs, fossil-based TPUs, and vulcanised rubbers (Fig. 6b),[30,38,60-67] and may be sustainable alternatives to those elastomers in various applications. For instance, soft EEL TPEE may be considered for cushioning and inflatable devices. LMM, LMH and LHM TPUs with medium hard hardness have potential in apparels and shoe soles.[68] Hard LIH, SIL, PUU and SML may be studied further for sealing and tubing with moderate flexibility.[69] Furthermore, the low T_gs make these biobased elastomers promising in insulation for cold-chain logistics, medical, industrial and automotives in sub-zero environments, etc.[31] The highly stretchable elastomers with low hysteresis may be useful for applications such as human motion sensors, soft actuators and soft robotics.[70] The elastomers with high strength, hardness and energy dissipation have potential in shock or vibration absorption, while those with low compression sets may find applications in gaskets and seals.[71] Specialty tests for each application should be performed to fully verify their applications.

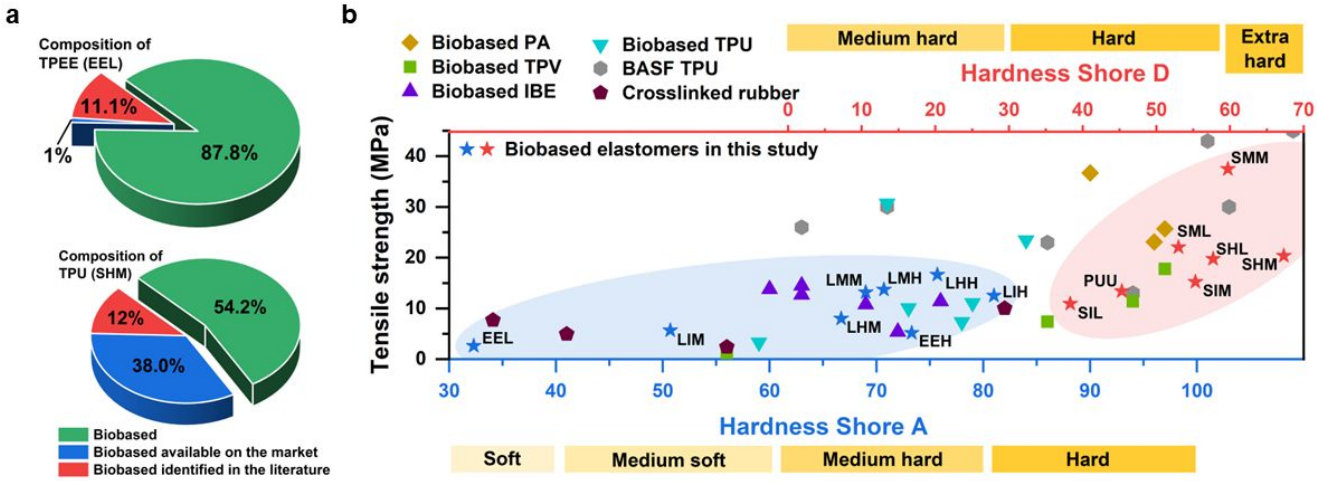

Fig. 6: Biobased content of the TPEs in this study and comparison of their properties with some existing elastomers. a, Compositions of the biobased TPEs prepared in this work. b, A scatter plot of biobased TPEs prepared in this work, in terms of Shore A (blue stars and circled area) or D (red stars and circled area) hardness and tensile strength, in comparison to some existing biobased elastomers (PA: polyamide,[30,38,60] TPV: thermoplastic vulcanizate[61], IBE: itaconate-based elastomers[62], and TPU[63]), commercial TPUs[32] and chemically crosslinked/vulcanised rubbers: EPDM (ethylene propylene diene monomer rubber),[64] PDMS (polydimethylsiloxane),[65] NBR (nitrile butadiene rubber)[66] and SBR (styrene butadiene rubber)[67].

Conclusions

Biobased polyether diols with 76 and 163 methylene groups (including tertiary carbons) on the main chains were successfully prepared using a green chemistry method, which addresses the challenge associated with the synthesis of polyethers containing more than five methylene groups from cyclic ethers. A biobased monomer derived from fatty acids was used with an organic catalyst to prepare the polyether diols with only water as the byproduct. Synthesis condition was readily adjustable to control their methylene groups and molecular weights.

Utilising the long-chain polyether diols as the soft segment, a series of TPUs were synthesised. By introducing aromatic, cycloaliphatic and molecular symmetry in their structure, a wide range of mechanical properties were achieved with hardness ranging between 50.7 (Shore A) and 67.3 (Shore D), as well as tensile strength and elongation at break up to 37.47 MPa and 995%. Their glass transition temperature as low as –51.4 °C ensures their performance in low temperature environments as elastomers. Processability of the sustainable elastomers was investigated by computational simulations with advanced viscoelastic models, and verified with industrial polymer processing techniques such as extrusion, injection moulding, and compression moulding completed to manufacture products with various shapes and dimensions. Chemical resistance, optical clarity and dyeability were also demonstrated.

The use of the long-chain polyether diols as a soft segment in TPEs is expandable and can be extended to other types of elastomers. In this study, PUU and TPEE types were explored, offering a wider performance range with softer mechanical properties and higher stretchability for the TPEE family. A kilogram scale of production of either polyether diols or TPEs was completed with a laboratory set up. Reprocessability and recyclability in the TPEs also benefit their sustainable manufacturing, together with the density of the TPEs lower than water density (0.90 – 0.99 g cm^{-3}) and biobased content as high as 87.8 wt.%.

The renewable ether-based thermoplastic elastomers investigated in this work have potential to replace some existing elastomers, in terms of comparable material performance and better sustainability. Specialty tests of TPEs (TPU, TPEE, and TPUU types) may be carried out in the future to fully assess their potential for chosen applications. The novel synthesis strategy reported here enables the sustainable production of ether-based polymers, with biobased long-chain polyether diols as their building blocks, offering a viable platform to design and manufacture thermoplastic elastomers with flexible molecular designs and controllable properties for diverse applications.

Experimental

Materials

A biobased diol under the tradename of Pripol™ 2030, with a composition of 1% of monomeric alcohol, 95% of dimer alcohol and 4% of trimer alcohol by weight, was supplied by Cargill. Antimony (III) oxide (Sb_2O_3, 99.99%), 1,4-butanediol (ReagentPlus®, ≥99%), curcumin (≥75%, with bisdemethoxycurcumin ≤5% and demethoxycurcumin ≤20%), 1,4-cyclohexanedimethanol (mixture of cis and trans, 99%), deuterated chloroform ($CDCl_3$, 99.8%), dibutyltin dilaurate (DBTDL, ≥96%), dimethyl terephthalate (ReagentPlus®, ≥99%), 1,6-hexamethlyenediamine (98%), imidazole (≥99.5%), isophorone diisocyanate (98%), 4,4′-methylenebis(cyclohexyl isocyanate) (90%), 4,4′-methylenebis(phenyl isocyanate) (98%), phenolphthalein (ACS reagent), phthalic anhydride (ACS reagent, ≥99%), *p*-toluenesulfonic acid (ACS reagent, ≥98.5%), pyridine (HPLC grade, ≥99.9%), sodium hydroxide (NaOH, ACS reagent, ≥97.0%), solvent green 3 (95%), tetrahydrofuran (THF, HPLC grade, ≥99.9%) and titanium(IV) n-butoxide (TBT, reagent grade, 97%) were purchased from Sigma-Aldrich.

Synthesis of long-chain polyether diols

A 2 L round bottom flask was purged by nitrogen thrice prior to use and equipped with an oil heating bath and mechanical stirrer (IKA HBR 4 Control). Pripol 2030 was charged into the flask and PTSA (3 mol% to Pripol 2030) was added. The reaction was performed at 180 °C for 7 h or 19 h with an agitation at 600 rpm under a flow of nitrogen. The water vapour generated by polycondensation was removed by a Dean-Stark apparatus first, followed by vacuum drying for the last 2 h of reaction.

Synthesis of ether-based thermoplastic polyurethane elastomers

First, hard segment intermediates were prepared by mixing a chosen diisocyanate (IPDI, MDI or HMDI) and the CHDM chain extender with DBTDL catalyst (0.05 % w/w to diisocyanate) in THF (30 % w/w) at 65 °C for 1 h. Secondly, the polyether diol and hard segment intermediates were mixed and their concentration in THF was adjusted to 40 % w/w. The reaction was performed at 65 °C for 3 h. The molar ratio of the polyether diol to diisocyanate to chain extender was varied. The resulting TPU elastomers were collected by pouring onto a non-sticky baking tray and dried in a fume cupboard at ambient temperature (20 ± 2 °C) for 24 h, followed by drying in a vacuum oven at 40 °C for 24 h.

Synthesis of ether-based thermoplastic polyurethane-urea elastomers

The polyether diol with 7 h of the synthesis time was mixed with HMDA at 65 °C, together with DBTDL catalyst (0.05 % w/w to diisocyanate). IPDI was added dropwise and the reaction continued for 4 min. The molar ratio of polyether diol, HMDA and IDPI was 1:1.67:3.5 (polyether diol:HMDA:IPDI). The resulting PUU elastomer was collected and dried in a vacuum oven for 24 h before use.

Synthesis of thermoplastic polyether-ester elastomers

For the synthesis of TPEE, BDO and DMT were used as the hard segment components. The polyether diol with 7 h of the synthesis time was added by BDO and DMT at molar ratios of 1:0.28:1.42 or 1:3.9:5.45 (polyether diol:BDO:DMT) together with Sb_2O_3 catalyst (0.1% w/w each to the total reactants). The [OH]/[COOH] molar ratio was kept at 1.10. The reaction temperature was raised from 140 °C to 220 °C at a ramp rate of 10 °C h^{-1} for 8 h, and kept at 220 °C for another 15 h. Subsequently, the temperature was increased to 240 °C, TBT catalyst was added (0.1% w/w each to the total reactants), and the reaction was continued further for 6 h. The polycondensation reaction was performed under a flow of nitrogen,

and water vapour generate from the reaction was removed by a Dean-Start apparatus, a cold trap and then vacuum drying. The resulting TPEE elastomers were collected and dried in a vacuum oven at 40 °C for 24 h before use.

Characterisation

Gel permeation chromatography was carried out on an Agilent 1260 Infinity II system with a refractive index detector. The eluent was THF with 2.0% v/v triethylamine and 0.05% w/v butylated hydroxytoluene inhibitor. Polystyrene standards (the peak molecular weight, M_p= 6570000, 3152000, 885000, 479200, 194500, 75050, 22790, 10330, 4880, 1210, 580 and 162 g mol^{-1}) were used for calibration. Samples were doubly filtered before the tests using polytetrafluoroethylene syringe filters (pore size = 0.45 µm).

^{1}H and ^{13}C nuclear magnetic resonance spectroscopy was conducted on a Bruker Avance AVIII spectrometer equipped with a 5 mm solution-state BBO probe with Z-gradient using $CDCl_3$ as the solvent at 25 °C. For ^{1}H NMR spectroscopy, a resonance frequency of 400.13 MHz, excitation pulse of 30°, acquisition points of 64 k, as well as spectral width of 20 ppm with 128 transients and 6 s relaxation delay were used. For ^{13}C NMR spectroscopy, a resonance frequency of 100.2 MHz was used with the carbon-13 coupled with proton decoupling (C13-CPD) method and a 30° excitation pulse program of zgpg30 pulse sequence (2048 transients, 240 ppm spectral width, 64 k FID size, 4 s recycle delay). The NMR spectra were normalised with an internal reference of tetramethylsilane. Attenuated total reflectance (ATR) Fourier transform infrared spectroscopy (FTIR) was performed on a Thermo Fisher Nicolet Apex with Smart iTX ATR accessory (500 – 4000 cm^{-1}, resolution: 2 cm^{-1}, and number of scans: 16). For solid samples, a pressure of 180 N was applied by a built-in screw to extend the degree of sample contact on the diamond ATR crystal. The FTIR spectra were normalised by the background measurements as the reference.

Differential scanning calorimetry was conducted between −80 and 200 °C at a rate of 10 °C min^{-1} under a nitrogen atmosphere (50 ml min^{-1}). A TA Instruments Discovery DSC25 equipped with a RCS90 refrigeration system was employed in this study. Small disc samples were prepared by punching (8.67 ± 1.03 mg). Two heating and cooling cycles were run with 2 min of isothermal between the cycles. The 2nd heating cycle was reported. Thermogravimetric analysis was carried out on a Perkin Elmer Pyris One between 25 to 800 °C at 10 °C min^{-1} under a nitrogen atmosphere (50 ml min^{-1}). The sample weights were 5.8 – 6.4 mg.

Quasi-static uniaxial tensile tests were performed at ambient temperature (21 ± 2 °C) following ISO 37. Dumbbell specimens (thickness: 2.04 ± 0.09 mm, n = 5) were cut from hot-pressed films using a cutting die (Ray-ran). A Lloyd LS5 mechanical tester equipped with a 500 N load cell was used at a crosshead speed of 200 mm min^{-1}. Cyclic tensile tests were performed between 0 and 100% strain for 100 cycles at a speed of 200 mm min^{-1} and ambient temperature using a Lloyd LRX mechanical tester equipped with a 50 N load cell. There was no extra recovery time between the cycles. The hysteresis ratio (h) at a certain cycle was calculated by equation (1).

$$h = 1 - \frac{e_d}{e_a} (1)$$

where e_d is the dissipated energy calculated by the area between the loading and unloading curves and e_a is the applied energy calculated by the area under the loading curve.

Compression set testing was done at ambient temperature according to ISO 815. Disk specimens (diameter: 12.7 ± 0.3 mm; thickness: 6.11 ± 0.02 mm; n = 3) were placed between rectangular stainless-steel plates with spacers (4.54 ± 0.01 mm). A thin coating of silicone-free lubricant (Brand 61610) was applied on the contact points between the disk specimens and the stainless-steel plates. Compression strain of 25.8 ± 0.2% was used according to the standard. At the specific time intervals of 24 and 72 h, the specimens were released and transferred to a bench to allow 30 min of recovery time. The thickness was then measured. The compression sets were calculated by equation (2), where t_0 is the initial thickness of the specimens, t_1 is the thickness after recovery, and t_s is the height of spacers.

$$Compression\ set = \frac{t_0 - t_1}{t_0 - t_s} \times 100\ (\%) (2)$$

Hardness was measured at ambient temperature according to ISO 48 with Shore type A and D indenters (Coats Machine Tool), with a test time of 15 s. The test pieces (thickness: 6.06 ± 0.19 mm) were prepared by a platen press (Collin P200P). The indentation points were at least 20 mm away from any edge of the specimens.

Computer simulation of elastomer extrusion process and die swell behaviour

Simulations were performed in ANSYS Polyflow using five mathematical models: generalised Newtonian, simplified viscoelastic, Giesekus, Phan-Thien Tanner and Pom-Pom. The last three are viscoelastic models. A material model was produced by importing the data from rheological testing as well as density into Polyflow. An extruder model was designed with a die of an internal diameter of 2.5 cm, and then meshed with the mesh consisting of 5534 nodes and 4298 elements, with a volume flow rate of 0.01106 cm^3 s^{-1} applied at the inlet. The outer surface of the polymer melt was treated as a free surface to allow for die swell to be shown. Die swell was calculated using the viscoelastic models by equation (3) where r_{melt} and r_{die} represent the radii of the melt and die respectively.

$$Die\ swell = \frac{r_{melt} - r_{die}}{r_{die}} x\ 100\% \quad (3)$$

Processing of ether-based TPU products

Elastomer powders were acquired by using a Rondol 6850 cryogenic mill with liquid nitrogen and used for the processing study below. Injection moulding was performed on a Ray-Ran Test Sample Injection Moulding Apparatus at 155 °C.

For processing of tubings, a twin-screw extruder (ThermoScientific Haake Polylab OS RheoDrive 7 assembled with Haake Rheomix OS PTW16) was equipped with a cooling line with calibrator, a feeder (Movacolor Micro MC18), a pulling/cutting unit (Dr. Collin RA 400) which pulled the product at a constant line speed and cut the parts to desirable lengths, a water cooling bath, as well as a laser scanning unit (BETA LaserMike, NDC Technologies) which measured the diameter of products. The inner diameter of the die and outer diameter of the pin was 8.2 mm and 2.1 mm, respectively. Tubes of three different diameters were obtained by applying different winding speeds. The setting temperatures are 125, 130, 140, 155,

View Article Online
DOI: 10.1039/D6GC00989A

155 and 135 °C for barrel zones 1 – 6 respectively within the extruder. Filaments were also manufactured with extrusion by using a die with a diameter of 4.0 mm. Elastomer pellets were obtained by pelletising the filaments using a pelletiser (ThermoScientific L-002-0424). Films were acquired by pressing the materials in a stainless-steel mould (thickness: 2 mm) at 155 °C using a platen press (Collin P200P).

Statistics

All measurements were reported as the mean ± standard deviation with a confidence level of 95%. Error bars indicate standard deviation of the means.

Author contributions

S.Y.: Methodology, investigation, data curation, formal analysis, writing – original draft; C.B.: data curation, formal analysis, writing – review & editing; J.J.C.B.: methodology, funding acquisition, writing – review & editing; P.J.M.: methodology, funding acquisition, writing – review & editing; B.C.: conception, methodology, formal analysis, funding acquisition, project administration, writing – original draft, writing – review & editing.

Conflicts of interest

There are no conflicts to declare.

Data availability

The authors have cited additional references within the Supplementary Information.
[72,73,74,75,76,77,78,79,80,81,82,83,84,85,86,87,88,89,90,91,92,93,94]

The dataset underpinning this article will be made available on Liverpool Elements for open access.

Acknowledgements

This work was supported by the Engineering and Physical Sciences Research Council of UK Research and Innovation [grant number EP/W018977/1]. Mark Billam and Graham Garrett from Queen's University Belfast are thanked for their help with polymer processing.

Notes and references

1 D. Babai, I. Pinkas, D. Naveh, R. Tenne. Polyetherimide (PEI) nanocomposite with WS2 nanotubes. *Nanoscale* 2024, *16*, 9917–9934.
2 J. Ling, W. Zhai, W. Feng, B. Shen, J. Zhang, W. Zheng. Facile preparation of lightweight microcellular polyetherimide/graphene composite foams for electromagnetic interference shielding. *ACS Appl. Mater. Interfaces* 2013, *5*, 2677–2684.
3 R. J. Spontak, N. P. Patel. Thermoplastic elastomers: fundamentals and applications. *Curr. Opin. Colloid. Interface Sci.* 2000, *5*, 333–340.
4 K. A. Chaffin, X. Chen, L. McNamara, F. S. Bates, M. A. Hillmyer. Polyether urethane hydrolytic stability after exposure to deoxygenated water. *Macromolecules* 2014, *47*, 5220–5226.
5 F. T. Hong, V. Ladelta, R. Guatam, S. M. Sarathy, N. Hadjichristidis. Polyether-Based Block Co(ter)polymers as Multifunctional Lubricant Additives. *ACS Appl. Polym. Mater.* 2021, *3*, 3811–3820.
6 A. Basterretxea, E. Gabirondo, C. Jehanno, H. Zhu, I. Flores, A. J. Müller, A. Etxeberria, D. Mecerreyes, O. Coulembier, H. Sardon. Polyether Synthesis by Bulk Self-Condensation of Diols Catalyzed by Non-Eutectic Acid-Base Organocatalysts. *ACS Sustain. Chem. Eng.* 2019, *7*, 4103–4111.
7 S. Pappuru, D. Chakraborty. Progress in metal-free cooperative catalysis for the ring-opening copolymerization of cyclic anhydrides and epoxides. *Eur. Polym. J.* 2019, *121*, 109276.
8 A. Diamanti, Z. Ganase, E. Grant, A. Armstrong, P. M. Piccione, A. M. Rea, J. Richardson, A. Galindo, C. S. Adjiman. Mechanism, kinetics and selectivity of a Williamson ether synthesis: Elucidation under different reaction conditions. *React. Chem. En.g* 2021, *6*, 1195–1211.
9 K. Ratzenböck, S. M. Fischer, C. Slugovc. Poly(ether)s derived from oxa-Michael polymerization: a comprehensive review. *Monatshefte fur Chemie* 2023, *154*, 443–458.
10 K. Ratzenböck, J. M. Uher, S. M. Fischer, D. Edinger, V. Schallert, E. Žagar, D. Pahovnik, C. Slugovc. Exploiting retro oxa-Michael chemistry in polymers. *Polym. Chem.* 2023, *14*, 651–661.
11 S. Zhang, A. Féret, H. Lefebvre, M. Tessier, A. Fradet. Poly(oxyalkylene) synthesis in Brønsted acid ionic liquids. *Chem. Comm.* 2011, 47, 11092–11094.
12 I. Flores. J. Demarteau, A. J. Müller, A. Etxeberria, L. Irusta, F.Bergman, C. Koning, H. Sardon. Screening of different organocatalysts for the sustainable synthesis of PET. *Eur. Polym. J.* 2018, *104*, 170–176.
13 S. Kaiho, A. A. R. Hmayed, K. R. D. Chiaie, J. C. Worch, A. P. Dove. Designing Thermally Stable Organocatalysts for Poly(ethylene terephthalate) Synthesis: Toward a One-Pot, Closed-Loop Chemical Recycling System for PET. *Macromolecules* 2022, *55*, 10628–10639.
14 M. Takenaka, Y. Kimura, H. Ohara. Influence of decomposition temperature of aromatic sulfonic acid catalysts on the molecular weight and thermal stability of poly(L-lactic acid) prepared by melt/solid state polycondenstaion. *Polymer (Guildf) 2018, 155*, 218–224.
15 T. Griggs, J. Ahmed, H. Majd, M. Edirisinghe, B. Chen. et al. A bio-based thermoplastic polyurethane with triple self-healing action for wearable technology and smart textiles. *Mater. Adv.* 2024, *5*, 6210–6221.
16 A. Sonseca, M. El Fray. Enzymatic synthesis of an electrospinnable poly(butylene succinate-co-dilinoleic succinate) thermoplastic elastomer. *RSC Adv.* 2017,*7*, 21258–21267.
17 Y. Nurhamiyah, A. Amir, M. Finnegan, E. Themistou, M. Edirisinghe, B. Chen. Wholly Biobased, Highly Stretchable, Hydrophobic, and Self-healing Thermoplastic Elastomer. *ACS Appl. Mater. Interfaces* 2021, *13*, 6720–6730.
18 J. R. Ernzen, C. H. Romoaldo, C. Gommes, J. A. Covas, A. Marcos-Fernández, R. Fiorio, O. Bianchi. Tuning Thermal, Morphological, and Physicochemical Properties of Thermoplastic Polyurethanes (TPUs) by the 1,4-Butanediol (BDO)/Dipropylene Glycol (DPG) Ratio. *Polymers (Basel)* 2022, *14*.

19 W. Lai, G. Wu. Reactive blending and transesterification-induced degradation of isosorbide-based polycarbonate blends. *Polym. Degrad. Stab.* 2019, *162*, 201–212 (2019).

20 Y. Tsai, L. Jheng, C. Hung. Synthesis, properties and enzymatic hydrolysis of biodegradable alicyclic/aliphatic copolyesters based on 1,3/1,4-cyclohexanedimethanol. *Polym. Degrad. Stab.* 2010, *95*, 72–78.

21 A. Mouren, L. Avérous. Aromatic thermoplastic polyurethanes synthesized from different potential sustainable resources. *Eur. Polym. J.* 2023, *197*, 112338.

22 D. J. Harris, R. A. Assink, M. Celina. NMR analysis of oxidatively aged HTPB/IPDI polyurethane rubber: Degradation products, dynamics, and heterogeneity. *Macromolecules* 2001, *34*, 6695–6700.

23 A. Kumar, A. P. M. Kentgens. Unravelling crosslinking and molecular structure in complex polyurethanes via advanced multinuclear solid-state NMR. *Polymer (Guildf)* 2025, *325*, 128245.

24 B. C. Smith. Infrared Spectroscopy of Polymers, IX: Pendant Ester Polymers and Polycarbonates. *Spectroscopy* 2022, *37*, 16-19.

25 M. Gorbunova, D. V. Anokhin, A. Abukaev, D. Ivanov. Impact of Soft Segment Composition on Phase Separation and Crystallization of Multi-Block Thermoplastic Polyurethanes Based on Poly(butylene adipate) Diol and Polycaprolactone Diol. *Crystals (Basel)* 2023, *13*, 1447.

26 M. Frydrych, S. Román, N. H. Green, S. MacNeil, B. Chen. et al. Thermoresponsive, stretchable, biodegradable and biocompatible poly(glycerol sebacate)-based polyurethane hydrogels. *Polym. Chem.* 2015, *6*, 7974–7987.

27 Y. S. Jung, J. Woo, E. Lee, S. Lee, E. J. Shin. Synthesis and properties of bio-based thermoplastic poly(ether urethane) for soft actuators. *J. Polym. Res.* 2022, *29*, 521.

28 [28] P. Kasprzyk, E. Glovińska, P. Parcheta-Swindowska, K. Rohde, J. Datta. Green TPUs from prepolymer mixtures designed by controlling the chemical structure of flexible segments. *Int. J. Mol. Sci.* 2021, *22*, 7438.

29 A. Das, P. Mahanwar. A brief discussion on advances in polyurethane applications. *Adv. Ind. Eng. Polym. Res.* 2020, *3*, 93–101.

30 Y. Nurhamiyah, G. Irvine, E. Themistou, B. Chen. Novel Biobased Polyamide Thermoplastic Elastomer with Medium Hardness. *Macromol. Chem. Phys.* 2021, *222*, 2100218.

31 L. B. Weaver, A. Batra, K. L. Walton. Thermoplastic Elastomer for Cold and Wet Applications. 2014.

32 N. Wingborg. Increasing the tensile strength of HTPB with different isocyanates and chain extenders. *Polym. Test.* 2002, *21*, 283–287.

33 M. Herrera, g. Matuschek, A. Kettrup. Thermal degradation of thermoplastic polyurethane elastomers (TPU) based on MDI. *Polym. Degrad. Stab.* 2002, 78, 323-331.

34 BASF. Elastollan® – Processing Recommendations. https://plastics-rubber.basf.com/emea/en/performance_polymers/products/ elastollan 2025 (accessed: 2025).

35 B. Wölfel, A. Seefried, V. Allen, J. Kaschta, C. Holmes, D. W. Schubert. Recycling and reprocessing of thermoplastic polyurethane materials towards nonwoven processing. *Polymers (Basel)* 2020, *12*, 1917.

36 Y. Zhang, Z. Feng, Q. Feng, F. Cui. Preparation and properties of poly(butylene terephthalate-co- cyclohexanedimethylene terephthalate)-b-poly(ethylene glycol) segmented random copolymers. *Polym. Degrad. Stab.* 2004, *85*, 559–570.

37 J. Dutta, K. Naskar. Investigation of morphology, mechanical, dynamic mechanical and thermal behaviour of blends based on ethylene vinyl acetate (EVA) and thermoplastic polyurethane (TPU). *RSC Adv.* 2014, *4*, 60831–60841.

38 Y. Nurhamiyah, B. Chen. Biobased polyamide 4,36 thermoplastic elastomer and its cellulose nanocomposites. *Macromol. Chem. Phys.* 2023, *224*, 2300013

39 Z. Czech, K. Agnieszka, P. Ragańska, A. Antosik. Thermal stability and degradation of selected poly(alkyl methacrylates) used in the polymer industry. *J. Therm. Anal. Calorim.* 2015, *119*, 1157–1161.

40 W. Pongdong, C. Kummerlöwe, N. Vennemann, A. Thitithammawong, C. Nakason. A Comparative Investigation of Rice Husk Ash and Siliceous Earth as Reinforcing Fillers in Dynamically Cured Blends of Epoxidized Natural Rubber (ENR) and Thermoplastic Polyurethane (TPU). *J. Polym. Environ.* 2018, *26*, 1145–1159.

41 C. Slater, C. Davis, M. Strangwood. Compression set of thermoplastic polyurethane under different thermal-mechanical-moisture conditions. *Polym. Degrad. Stab.* 2011, *96*, 2139–2144.

42 F. A. Martins, L. A. Santos, D. R. Silva, C. F. Guerra, F. M. Bickelhaupt, M. P. Freitas. Iodine Gauche Effect Induced by an Intramolecular Hydrogen Bond. *J. Org. Chem.* 2022, *87*, 11625–11633.

43 H. H. Winter, M. Mours. Rheology of Polymers Near Liquid-Solid Transitions. in *Neutron Spin Echo Spectroscopy Viscoelasticity Rheology* 1997, *134*, 165–234.

44 B. Pukánszky, K. Bagdi, K. Molnár, B. Pukannszky. Thermal analysis of the structure of segmented polyurethane elastomers: Relation to mechanical properties. *J. Therm. Anal. Calorim.* 2009, *98*, 825–832.

45 W. J. Xu, J. J. Wang, Shi. Y. Zhang, J. Sun, C. X. Qin, L. X. Dai. Tuning chain extender structure to prepare high-performance thermoplastic polyurethane elastomers. *RSC Adv.* 2018, *8*, 20701–20711.

46 G. Bishko, T. C. B. McLeish, O. G. Harlen, R. G. Larson. Theoretical Molecular Rheology of Branched Polymers in Simple and Complex Flows: The Pom-Pom Model. *Phys. Rev. Lett*. 1997, *79*, 2352–2355.

47 J. Tichy, B. Bou-Saïd. The Phan-Thien and Tanner Model Applied to Thin Film Spherical Coordinates: Applications for Lubrication of Hip Joint Replacement. *J. Biomech. Eng.* 2008, *130*, 021012.

48 H. Giesekus. A simple constitutive equation for polymer fluids based on the concept of deformation-dependent tensorial mobility. *J. Nonnewton Fluid. Mech.* 1982, *11*, 69–109.

49 K. Y. Pérez-Salas, E. L. García-Romero, A. A. Barrientos-Cruz. Elastic and shear-thinning effects in contraction flows: a comparison. *Rheol. Acta* 2024, *63*, 585–601.

50 C. Abeykoon, A. L. Kelly, E. C. Brown, J. Vera-Sorroche, P. D. Coates, E. Harkin-Jones, K. B. Howell, J. Deng, K. Li, M. Price. Investigation of the process energy demand in polymer extrusion: A brief review and an experimental study. *Appl. Energy* 2014, *136*, 726–737.

51 J. Y. Kim, E. S. Seo, D. S. Park, K. M. Park, S. W. Kang, C. H. Lee, S. H. Kim. Chemical Modification of Isotactic Polypropylene by Melt Blending. *Fiber. Polym.* 2003, *4*, 107–113.

52 J. P. Sullivan, M. McManaway. Reinforced Elastomers. Patent US20110206878A1 (2011).

53 P. Steffanut, M. Sidqi, E. Dongiovanni, J. Abrahmi. Catalyst Composition For A Polyester Manufacturing Process. Patent US20170283548A1 2017.

54 S. J. Buwalda, P. J. Dijkstra, L. Calucci, C. Forte, J. Feijen. Influence of amide versus ester linkages on the properties of eight-armed PEG-PLA star block copolymer hydrogels. *Biomacromolecules* 2010, *11*, 224–232.

55 K. P. Rieser. BASF obtains long-term access to bio-based 1,4-butanediol QIRA. *BASF News Release* https://www.basf.com/global/en/media/news-releases/2023/09/p-23-306 2023 (accessed: 2025).

56 J. J. Lee, G. A. Kraus. One-pot formal synthesis of biorenewable terephthalic acid from methyl coumalate and methyl pyruvate. *Green Chem.* 2014, *16*, 2111–2116.
57 N. Kasmi, M. Majdoub, G. Z. Papageorgiou, D. N. Bikiaris. Synthesis and crystallization of new fully renewable resources-based copolyesters: Poly(1,4-cyclohexanedimethanol-co-isosorbide 2,5-furandicarboxylate). *Polym. Degrad. Stab.* 2018, *152*, 177–190.
58 H. YE. BASF in Korea starts to supply biomass balanced MDI, paving the way for a sustainable MDI value chain. *BASF News Release.* https://www.basf.com/in/en/media/news-releases/asia-pacific/2023/10/basf-in-korea-starts-to-supply-biomass-balanced-mdi--paving-the- 2023 (accessed: 2025).
59 G. Ferrara, T. P. Meloy. Low Dense Media Process: A New Process for Low-Density Solid Separation. Powder Technol. 1999, 103, 151–155.
60 L. Harley, Z. Rahmatpanah, B. Chen. Preparation and Characterization of Biobased Polyamide36,10 Elastomer and Its Foam. *Macromol. Mater. Eng.* 2025, *310*, e00129.
61 H. Kang, X. Hu, M. Li, L. Zhang, Y. Wu, N. Ning, M. Tian. Novel biobased thermoplastic elastomer consisting of synthetic polyester elastomer and polylactide by in situ dynamic crosslinking method. *RSC Adv.* 2015, *5*, 23498–23507.
62 H. Yang, H. Ji, X. Zhou, W. Lei, L. Zhang, R. Wang. Design, Preparation, and Evaluation of a Novel Elastomer with Bio-Based Diethyl Itaconate Aiming at High-Temperature Oil Resistance. *Polymers (Basel)* 11, 1897 (2019).
63 Y. S. Jung, J. Woo, E. Lee, S. Lee, E. J. Shin. Synthesis and properties of bio-based thermoplastic poly(ether urethane) for soft actuators. *J. Polym. Res*. 29, 521 (2022).
64 Z. Li, Z. Chen, W. Sun, Y. Liu, X. Wang, J. Lin, J. Wang, S. He. High-performance EPDM/organoclay nanocomposites by melt extrusion. *Appl. Clay Sci.* 2008, *40*, 38–44.
65 S. Wu, S. Peng, C. H. Wang. Stretchable strain sensors based on PDMS composites with cellulose sponges containing one- and two-dimensional nanocarbons. *Sens. Actuators A* 2018, *279*, 90–100 (2018).
66 X. Cao, C. Xu, Y. Wang, Y. Liu, Y. Liu, Y. Chen. New nanocomposite materials reinforced with cellulose nanocrystals in nitrile rubber. *Polym. Test.* 2013, *32*, 819–826.
67 A. Zanchet, L. N. Carli, M. Giovanela, J. S. Crespo, C. H. Scuracchio, R. C. R. Nunes. Characterization of Microwave-Devulcanized Composites of Ground SBR Scraps. *J. Elastomers Plast.* 2009, *41*, 497–507.
68 M. C. Iacob, D. Popescu, A. T. George. Printability of Thermoplastic Polyurethane with Low Shore A Hardness in the Context of Customized Insoles Production. *U.P.B. Sci. Bull. D* 2024, *86*, 95–106.
69 S. H. Jeon, J. E. Jeong, S. Kim, S. Jeon, J. W. Choung, I. Kim. Hardness modulated thermoplastic poly(Ether ester) elastomers for the automobile weather-strip application. *Polymers (Basel)* 2021, *13*, 525.
70 B. Huang, Z. Lv, M. Zhang, J. Liu, H. Liu, T. Li, L. Fu, B. Lin, C. Xu. Low mechanical-hysteresis soft materials: materials, design, and applications. *J. Mater. Chem. A* 2025, *13*, 15427–15452.
71 A. G. Akulichev, B. Alcock, A. T. Echtermeyer. Elastic recovery after compression in HNBR at low and moderate temperatures: Experiment and modelling. *Polym. Test.* 2017, *61*, 46–56.
72 J. Ren, L. Zhu, X. Zhang, Y. Luo, X. Zhong, B. Li, Y. Wan, K. Zhang. Variation characteristics of acid rain in Zhuzhou, Central China over the period 2011-2020. J. Environ. Sci. 2024, *138*, 496–505.
73 J. Tarun, J. Susan, J. Suria, V.J. Susan, S. Criton. Evaluation of pH of bathing soaps and shampoos for skin and hair care. Indian J. Dermatol. 2014, *59*, 442–444.
74 K. R. Hinga, Effects of pH on coastal marine phytoplankton. Marine Ecol. Prog. Ser. 2002, *238*, 281–300.
75 R. Vaid, E. Yildirim, M.A. Pasquinelli, M.W. King. Hydrolytic degradation of polylactic acid fibers as a function of pH and exposure time. Molecules 2021, *26*, 7554.
76 C.N. Ward, P.E. LeBlanc, R.E. Burrell. Effects of composition and pH on the degradation of hyaluronate and carboxymethyl cellulose gels and release of nanocrystalline silver**.** J. Appl. Biomater. Funct. Mater. 2024, *22,* 22808000241257124
77 N. Stachowiak. J. Kowalonek, j. Kozlowska, A. Burkowska-But. Stability studies, biodegradation tests, and mechanical properties of sodium alginate and Gellan gum beads containing surfactants. Polymers 2023, *15*, 2568.
78 R. K Chalasani, S. Dewasthale, E. Hablot, S. Shi. A Spectroscopic Method for Hydroxyl Value Determination of Polyols. *JAOCS, Journal of the American Oil Chemists' Society* 2013, *90*, 1787–1793.
79 M. Sokołowska, E. Stachowska, M. Czaplicka, M. El Fray. Effect of enzymatic versus titanium dioxide/silicon dioxide catalyst on crystal structure of 'green' poly[(butylene succinate)-co-(dilinoleic succinate)] copolymers. *Polym. Int.* 2021, *70*, 514–526.
80 J. Skrobot, W. Ignaczak, M. El Fray. Hydrolytic and enzymatic degradation of flexible polymer networks comprising fatty acid derivatives. *Polym. Degrad. Stab.* 2015, *120*, 368–376.
81 Y. Nurhamiyah, S. Yoon, B. Chen. Wholly Biobased Polyamide Thermoplastic Elastomer-Cellulose Nanocomposites. *Macromol. Mater. Eng.* 2022, *307*, 2200120.
82 N. S. Vrandečić, M. Erceg, M. Jakić, I. Klarić. Kinetic analysis of thermal degradation of poly(ethylene glycol) and poly(ethylene oxide)s of different molecular weight. *Thermochim. Acta* 2010, *498*, 71–80.
83 S. Yoon, B. Chen. Biomimetic Elastomer-Clay Nanocomposite Hydrogels with Control of Biological Chemicals for Soft Tissue Engineering and Wound Healing. *ACS Appl. Bio. Mater.* 2025, *8*, 2492–2505.
84 M. Alves. Carbon dioxide and vegetable oil for the synthesis of biobased polymer precursors. PhD thesis, Universit´e de Bordeaux 2016.
85 K. Schmidt-Rohr, J.-D. Mao, D.C. Olk, J. M. Bremner. Nitrogen-Bonded Aromatics in Soil Organic Matter and Their Implications for a Yield Decline in Intensive Rice Cropping. *PNAS* 2004, *101*, 6351–6354.
86 M. A. Gorbunova, E. V. Komov, L. Y. Grunin, M. S. Ivanova, A. F. Abukaev, A. M. Imamutdinova, D. A. Ivanov, D. V. Anokhin. The effect of separation of blocks on the crystallization kinetics and phase composition of poly(butylene adipate) in multi-block thermoplastic polyurethanes. *Phys. Chem. Chem. Phys.* 2022, *24*, 902–913.
87 P. X. Thinh, C. Basavaraja, D. G. Kim, D. S. Huh. Characterization and electrochemical behaviors of honeycomb-patterned poly(N-vinylcarbazole)/polystyrene composite films. *Polym. Bull.* 2012, *69*, 81–94.
88 B. B. Yilma, J. F. Luebben, G. Nalankilli. The Effect of Air, Ar and O2 Plasmas on the Electrical Resistivity and Hand-Feel Properties of Polyester/Cotton Blend Fabric. *Fibers* 2020, *8*, 17.
89 M. Reinecker, V. Soprunyuk, M. Fally, A. Sánchez-Ferrer, W. Schranz. Two glass transitions of polyurea networks: Effect of

View Article Online
DOI: 10.1039/D6GC00989A

the segmental molecular weight. *Soft Matter* 2014, *10*, 5729–5738.
90 M. Nofar, E. Büşra Küçük, B. Batı. Effect of hard segment content on the microcellular foaming behavior of TPU using supercritical CO_2. *J. Supercrit. Fluids* 2019, *153*, 104590.
91 B. D. Akkoyun, A. A. Wis, R. Yıldırım, Ü. Makal, G. Özkoç, M. Kodal. Enhanced Crystallinity Through Melt Annealing of Thermoplastic Polyurethanes. *J. Appl. Polym. Sci.* 2024, **142**, e56593.
92 M. S. S. Sadeghian, A. Raisi. A thermodynamic study on relationship between gas separation properties and microstructure of polyurethane membranes. *Sci. Rep.* 2023, **13**, 6038.
93 T. L. Chantawansri, Y. R. Sliozberg, J. W. Andzelm, A. J. Hsieh. Coarse-grained modeling of model poly(urethane urea)s: Microstructure and interface aspects. *Polymer (Guildf)* 2012, **53**, 4512–4524.
94 A. Martínez De Ilarduya, S. Muñoz-Guerra. Chemical structure and microstructure of poly(alkylene terephthalate)s, their copolyesters, and their blends as studied by NMR. *Macromol. Chem. Phys.* 2014, **215**, 2138–2160.

View Article Online
DOI: 10.1039/D6GC00989A

Data availability

The authors have cited additional references within the Supplementary Information.
[72,73,74,75,76,77,78,79,80,81,82,83,84,85,86,87,88,89,90,91,92,93,94]

The dataset underpinning this article will be made available on Liverpool Elements for open access.